Surface & Coatings Technology 436 (2022) 128293

Contents lists available at ScienceDirect

Surface & Coatings Technology

journal homepage: www.elsevier.com/locate/surfcoat

Thin film nanostructuring at oblique angles by substrate patterning

S. Muñoz-Piña [a], A.M. Alcaide [b], B. Limones-Ahijón [c], M. Oliva-Ramírez [b,d], V. Rico [b], G. Alcalá [e], M.U. González [c], J.M. García-Martín [c], R. Alvarez [b,f,*], D. Wang [g], P. Schaaf [g], A. R. González-Elipe [b], A. Palmero [b,**]

[a] Nano4Energy SLNE, C/Jose Gutiérrez Abascal 2, 28006 Madrid, Spain
[b] Instituto de Ciencia de Materiales de Sevilla (CSIC-US), Américo Vespucio 49, 41092 Seville, Spain
[c] Instituto de Micro y Nanotecnología, IMN-CNM, CSIC (CEI UAM + CSIC), Isaac Newton 8, 28760 Tres Cantos, Madrid, Spain
[d] Departamento de Física Atómica, Molecular y Nuclear, Universidad de Sevilla, Avda. Reina Mercedes, 41012 Seville, Spain
[e] Departamento Ingeniería Química y Materiales, Universidad Complutense de Madrid, Avenida Complutense s/n, Facultad de Ciencias Químicas, 28040 Madrid, Spain
[f] Departamento de Física Aplicada I, Escuela Politécnica Superior, Universidad de Sevilla, c/Virgen de África 7, 41011 Seville, Spain
[g] TU Ilmenau, Institute of Materials Science and Engineering and Institute of Micro- and Nanotechnologies MarcoNano®, Gustav-Kirchhoff-Str. 5, 98693 Ilmenau, Germany

ARTICLE INFO

Keywords:
Magnetron sputtering
Nanostructured thin films
Substrate patterning
Oblique angle deposition
Porous thin films

ABSTRACT

It is demonstrated that, besides classical nanocolumnar arrays, the oblique angle geometry induces the growth of singular structures in the nanoscale when using wisely designed patterned substrates. Well-ordered array of crosses, cylindrical nanorods or hole structures arranged in square or hexagonal regular geometries are reported as examples, among others. The fundamental framework connecting substrate topography and film growth at oblique angles is presented, allowing the use of substrate patterning as a feasible thin film nanostructuring technique. A systematic analysis of the growth of TiO_2 thin films on 4 different lithographic patterned substrates in 4 different scale lengths is also presented. A first conclusion is the existence of a height-based selective growth in the initial stages of the deposition, by which the film preferentially develops on top of the tallest substrate features. This behavior is maintained until the film reaches a critical thickness, the so-called Oblivion Thickness, above which the film topography becomes gradually independent of the substrate features. A general formula relating the spatial features of the pattern, the coarsening exponent and the Oblivion Thickness has been deduced.

1. Introduction

Last decades have witnessed the introduction of important modifications in well-established thin film deposition methodologies aiming to widen their nanostructuration possibilities and make them more versatile [1–3]. This is the case of the so-called plasma-assisted magnetron sputtering technique, a classical Physical Vapor Deposition (PVD) procedure that relies on the interaction between a plasma and a solid target to sputter species from the latter that, upon deposition, make the thin film grow [4]. In the classical configuration, the substrate is placed parallel to the target, resulting in the deposition of well-known dense and compact homogeneous layers [5–7]. However, if the substrate is tilted, in a so-called Oblique Angle configuration, a wide range of new possibilities emerge, enabling the growth of layers formed by nanocolumnar structures for tilt angles above a threshold value [8]. These nanostructured films have found applications in fields as different as sensors, biomedicine, microfluidics and plasmonics, to name a few, [9–18] thanks to their unique morphological features, e.g. high specific surface, tunable density, high porosity or high pore connectivity [19–21], which have motivated an intensive research to attain precise nanostructural control and optimum functionality. The aim of this paper is to demonstrate the profound connection between substrate topography and film growth when operating at oblique angles, as well as deducing the main principles describing the interplay between these elements. In this way, and based on the large number of reported possibilities, it is suggested that substrate patterning methods may effectively act as a feasible thin film nanostructuring technique.

In general terms, the oblique incidence of ad-species on a substrate

* Correspondence to: R. Alvarez, Instituto de Ciencia de Materiales de Sevilla (CSIC-US), Américo Vespucio 49, 41092 Seville, Spain.
** Corresponding author.
E-mail addresses: ralvarezmol@us.es (R. Alvarez), alberto.palmero@csic.es (A. Palmero).

https://doi.org/10.1016/j.surfcoat.2022.128293
Received 22 December 2021; Received in revised form 6 February 2022; Accepted 24 February 2022
Available online 1 March 2022

induces the so-called surface shadowing mechanism and the appearance of shadowed regions, i.e. parts of the growing surface where the deposition is inhibited due to the presence of mounds that capture most ad-species [22]. This causes a surface selective and competitive development that ends up in the formation of tilted nanocolumnar structures separated by large pores [8]. Consequently, the nanocolumns are always found in the form of large arrays with strongly interdependent heights. The main experimental control parameters defining the columnar development in oblique angle depositions with magnetron sputtering (MS-OAD) are the tilt angle of the substrate with respect to the target, α, and the working pressure in the deposition reactor [23]. While the former defines the angle of incidence of ad-species and the efficiency of the surface shadowing mechanisms, the latter influences the transport of sputtered species in the plasma from the target to the substrate. In this way, at very low pressures (or, likewise, for large mean free paths of deposition particles in the plasma gas) the sputtered species move according to a ballistic diffusive regime from the target to the film, while at very high pressures (short mean free paths) their movement becomes Brownian-like due to the large amount of collisions with heavy plasma species, thus arriving at the substrate along any possible angular direction. In real conditions, both types of transports coexist depending on the target-film distance and the mean free path value [24]. Different characteristic film morphologies have been reported when the growth takes place on a flat substrate and at relatively low pressures: compact (when $\alpha < 60°$), compact with tilted mesopores that percolate from the top of the film to the very substrate (when $60° \lesssim \alpha \lesssim 80°$), and tilted nanocolumnar structures (when $\alpha \gtrsim 80°$). Moreover, at relatively high pressures, sponge-like vertically aligned and coalescent structures are promoted, no matter the tilt angle of the substrate, due to the non-preferential arrival of sputtered species along any specific oblique direction [23].

The influence of both, deposition pressure and α, has been thoroughly studied in the literature for numerous materials and conditions (see for instance refs. [23,25–27] and references therein). Yet, to our knowledge, no systematic study has appeared analyzing the interplay between the film columnar arrangement and the topography of the substrate at oblique geometries. Indeed, it is known that any pattern carved on the substrate strongly modifies the surface shadowing mechanisms and affects the resulting film nanostructure: in ref. [28], for instance, it was found that the morphology of a SiO_2 thin film grown by MS-OAD on a 1D rippled surface tends to mimic the ripples' features, up to a critical thickness, called *Oblivion Thickness*, Δ_O, above which the pattern progressively vanishes from the film surface. Moreover, in ref. [29] these results where corroborated by growing W thin films on different stainless-steel polished substrates by MS-OAD, finding that the nanocolumnar arrangement mimicked the substrate topographical features up to a film thickness of few microns, above which the film surface started to evolve independently of such features. These ideas were also tested using as substrates the self-arrangement of nanosphere beads on a surface [30], alumina [31–40] or porous silicon membranes [41,42], finding that the nanocolumnar films replicate the main features of these substrate patterns for small film thicknesses. Remarkably, this substrate-driven nanostructuring mechanism has been applied just relying on an empirical basis, without any well-founded general formulation describing the interplay between the substrate geometrical features and the nanocolumnar growth. This is the scope of this work, to theoretically and experimentally develop some basic principles by which the aforementioned phenomenology can be rationalized. For this study numerous depositions have been carried out on 4 different periodic patterned substrates in 4 different scale lengths, below and in the order of 1000 nm. For simplicity, and due to the large number of potential applications based on it, TiO_2 has been employed, although the results are widely applicable to other materials.

2. Fundamentals of thin film growth on patterned substrates at oblique angles

In this section, some fundamental principles of MS-OAD when the substrate topography is tailored according to a certain pattern are discussed. For this purpose, a well-tested model of the deposition has been used. This model has been successfully applied in numerous cases for oxides and metal thin films grown by MS-OAD on flat substrates, and its details can be checked in refs. [23,28]. For instance, as a case example, in Fig. 1a–b the cross-sectional and top views, respectively, of a simulated film grown under the experimental conditions of this paper on a flat substrate for a film thickness of 300 nm are presented. There, it is evident the existence of tilted and well-separated nanocolumnar structures whose tips can be seen at the top-view image in Fig. 1b. This model was used to determine which particular geometrical feature of a given substrate pattern gives rise to the nanocolumnar arrangement. To do so, simulations were run on substrates formed by numerous coalescent rectangular prism-shaped platforms, with different base area and height defining their topography. Consequently, the particular geometrical aspect of these platforms that may prompt a faster/slower vertical development during the early stages of growth could be identified. The followed procedure is described next:

- A substrate with a lateral size of 250 nm was formed by coalescing several platforms with random base area and height (see Fig. 2a for an example).
- For a given substrate, and under the experimental conditions described in the experimental setup section, the deposition of an individual atom was simulated and the particular location where it landed on the substrate was calculated.
- The features of the landing location (base area and height of the platform) were saved for statistical purposes, after which the deposited atom was removed from the simulation to maintain steady substrate topography. Only the atoms deposited on the top surface of the platforms were considered to contribute to the vertical growth. This process was repeated for a total amount of 10^8 atoms.
- For a given substrate, similar statistics were performed assuming different angles of incidence of deposition species.
- The process described above was carried out using 10^4 different randomly generated substrates containing different configurations of platforms.

The representation of the vertical growth rate per unit area as a function of the area of the base of the platform, irrespective of height, and for different angles of incidence (see Supplementary figure S1), indicates that the vertical growth rate does not depend on the size of the base: in other words, the area of the base of the platforms does not play a role in determining how faster or slower the vertical development of the platform is. In addition, the plots in Fig. 2b, corresponding to the vertical growth rate per unit area as a function of height, irrespective of the area of the base, depict a clear trend: in classical non-oblique depositions (angle of incidence of 0°), Fig. 2b indicates that the growth rate is independent of the height of the platform. Yet, as soon as the incidence is oblique, a clear preferential growth of taller platforms is found in detriment of lower ones. This has been checked for different pattern geometries finding similar results for 1D walls or cylinders instead of rectangular prims (results not shown). This numerically demonstrates a general rule, that from now forth we dub the height-based selective growth principle, by which *the taller certain geometrical elements are on the substrate, the faster they will vertically develop in the initial stages of growth*, implying that the nanocolumns will initially arrange according to the tallest features of the substrate pattern. Yet, it is noteworthy that, according to Fig. 2b, the more oblique the incidence is, the more selective the growth becomes and, hence, the criterion by which a certain feature is tall enough or not to develop would depend on the angle of incidence of the deposition species. In practical conditions, where the

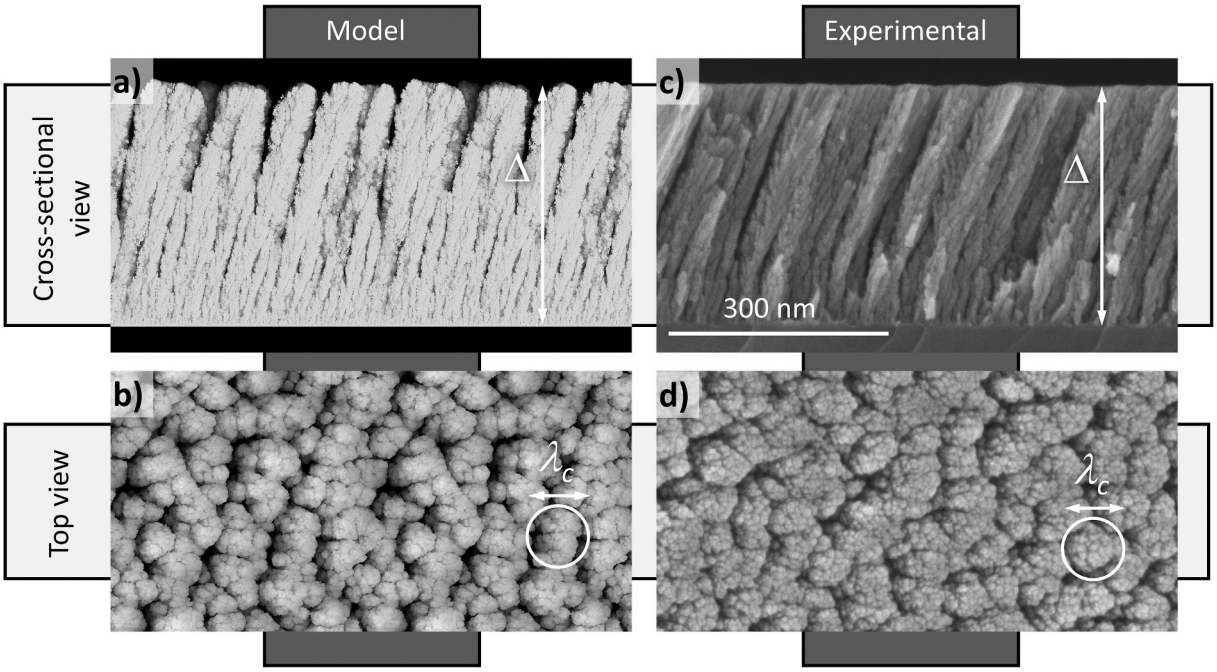

Fig. 1. Cross-sectional and top view images of a film deposited on a flat surface under the experimental conditions of this paper. a) Simulation. b) Experimental. The characteristic length of the film features, λ_c, and the film thickness, Δ, are also depicted.

incidence is defined by a probability distribution [2], this means that, for a given substrate pattern and in the absence of any further detail on the growth conditions, the proposed principle only provides qualitative information on key pattern elements, especially when these show large dispersion of heights or smooth slopes (see the Results and discussion section for more details on this issue).

The height-based selective growth principle sheds some light on the connection between substrate features and thin film morphology at oblique geometries during the first stages of growth. Interestingly, this principle is implicitly assumed in many works in the literature using the concept of shadowed region (i.e. the area behind each mound where the deposition is inhibited thanks to the shadowing mechanism), which takes into account that the larger this region is, the more atoms would be deposited on the mound that casts the shadow and, thus, the faster it will develop [8]. In this regard, both aspects, the height of a certain mound and the size of the shadowed region, can be taken as equivalent for our purposes, as both quantities are proportional. To our knowledge, the height-based selective growth principle deduced herein has not been quantitatively demonstrated in the literature before, nor the particular morphological aspect defining its efficiency.

Once the height-based selective growth principle is established, the subsequent film development on a patterned substrate for increasing thicknesses is discussed. Here, it is important to notice that, upon growth, the nanocolumns increase their diameter and merge, forming either larger nanocolumns or closely-packed clusters of nanocolumns. This process introduces a characteristic length in the plane of the substrate, λ_c, that relates to the size of these features that grow as a whole and not as independent elements (see Fig. 1b and d for a visual representations of λ_c). Consequently, the film development on a patterned substrate implies the accommodation of such features, defined by λ_c, into those defining the pattern. λ_c can be calculated by analyzing the growth on a flat substrate, i.e. in the absence of any other relevant characteristic lengths, using the concept of correlation length, a statistical quantity that, given a surface topography, can be obtained through different statistical methods, e.g. Fourier or surface self-correlation analyses [43]. Remarkably, λ_c is known to increase with film thickness, Δ, as a power law

$$\lambda_c = C\Delta^{1/z}, \tag{1}$$

where C is a proportionality constant and $1/z$ the so-called coarsening exponent. Both C and $1/z$ are process- and material-dependent quantities that, together with the growth and roughness exponents, characterize the film growth [43,44] (for simplicity, an isotropic behavior was assumed for λ_c).

According to the ideas above, the comparison between λ_c and the typical lengths defining the pattern determines the different stages of growth, which are described next (in the audiovisual information of this manuscript we present a video that illustrates these stages):

- In agreement with the height-based selective growth principle above, in the initial stages of growth, the film surface tends to mimic the pattern defined by the tallest substrate elements.
- For increasing thicknesses, the nanocolumnar arrangement at the edges of tallest regions will spread towards contiguous lower regions, progressively covering them, at a pace defined by λ_c. In this way, if λ_{min} is the shortest length between the tallest elements of the pattern, the Oblivion Thickness, Δ_o, introduced as the critical thickness above which the pattern starts to vanish from the film surface, would be defined by the condition $\lambda_c(\Delta_o) \sim \lambda_{min}$, which using Eq. (1) yields the relation

$$\Delta_o \sim \left(\frac{\lambda_{min}}{C}\right)^z, \tag{2}$$

that links three key quantities: Δ_o, λ_{min} and the coarsening exponent, z.

- As the film develops, columns will continue to spread over the surface, progressively covering the different valleys between taller surface features. If λ_{max} is the longest characteristic length between these features, the critical thickness above which they will no longer be visible from the film surface, Δ_{FG}, can be similarly found when $\lambda_c(\Delta_{FG}) \sim \lambda_{max}$, which using Eq. (1) results in

$$\Delta_{FG} \sim \left(\frac{\lambda_{max}}{C}\right)^z \tag{3}$$

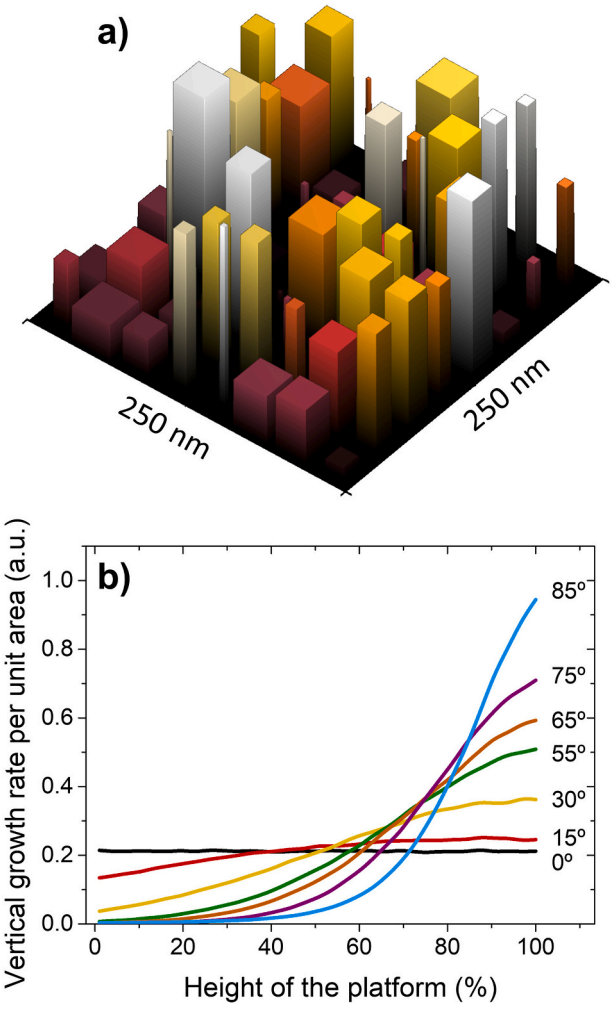

Fig. 2. a) Example of a substrate employed for the simulations. The pattern is formed by coalescent platforms with the shape of rectangular prisms with random base area and height. For a better visual appreciation, the platforms are presented in different colors. b) Calculated vertical growth rate per unit area as a function of the height of the platform (height percentage calculated with respect to the maximum value).

In agreement with ref. [28], this growth stage is denoted as free growth regime.

When there is only one characteristic length separating the tallest parts of the pattern, $\lambda_{min} = \lambda_{max} = \lambda_0$, Δ_o coincides with Δ_{FG}. Moreover, dividing Eq. (2) by Eq. (3) gives a general relation between the pattern features and the two critical film thicknesses as

$$\frac{\Delta_o}{\Delta_{FG}} \sim \left(\frac{\lambda_{min}}{\lambda_{max}}\right)^z, \tag{4}$$

an expression that connects the geometrical features of the pattern, the critical thicknesses defining the different growth stages and the coarsening exponent characterizing the nanocolumnar growth.

At this point it is important to note that Eq. (2) is formally equal to an empirical equation found in ref. [28] through a numerical fit. There, the growth of a SiO_2 thin film by MS-OAD was analyzed when the substrate contained a sinusoidal pattern with wavelength λ, finding the relation $\Delta_0 \propto \lambda^\gamma$ with $\gamma = 1.55 \pm 0.04$ under those deposition conditions. Remarkably, by considering that the distance between the lower parts of the sinusoidal pattern is $\sim\lambda/2$, the comparison with Eq. (2) gives away the relation $\gamma = z$. Unfortunately, the value of z was not specifically calculated in ref. [28] under their conditions, precluding a direct comparison with the calculated value of γ. Yet, this parameter could be easily obtained using the data displayed in Fig. 2a in the same publication, finding $z = 1.53$, which compares fairly well with the fitted value of γ.

Based on the discussion above, a general framework describing the influence of a given substrate pattern on the growth of a nanocolumnar thin film at oblique geometries has been developed. In this way, the vertical and horizontal dimensions of the geometrical elements defining the substrate pattern affect the growth very differently: while the vertical ones (heights) define the initial stages of growth and the regions of preferential vertical development, the typical horizontal distances (in the plane of the substrate) define the subsequent columnar development and the Oblivion and Free Growth Thicknesses. As a final comment, it is important to underline that for simplicity an isotropic behavior has been assumed for λ_c. However, the presented ideas can be easily generalized to anisotropic conditions, by solely considering the power law defined by λ_c in the particular direction that connects two contiguous tallest surface features.

3. Experimental setup

TiO_2 thin films were grown in a semi-industrial scale reactor that operates at the company Nano4Energy SLNE. The target is rectangular with a size 20 × 7.5 cm^2 with a balanced magnetic configuration, exhibiting a racetrack with the shape of a rectangle (the long and short sides being 13.5 and 4.2 cm, respectively) with lines that are about 3 mm wide. The base pressure in the reactor was 2×10^{-6} mbar. The DC electromagnetic signal to maintain the plasma was generated by a Pinnacle Generator source set at 400 W and current intensity of 1 A, being the argon and oxygen fluxes 18.1 and 2.5 sccm respectively, and the total deposition pressure 3.3×10^{-3} mbar. The OAD configuration was achieved as described in reference [45]: the substrate holder was located 10 cm away from the target and parallel to it, while the substrate was placed perpendicular to both, in such a way that atoms stemming from the racetrack may reach the substrate along an averaged oblique angle of ~80° (a scheme of the reactor is shown in Fig. 3). As demonstrated in ref. [45], this configuration ensures that both momentum and kinetic energy distributions of sputtered species deposited at the substrate coincide with those found in laboratory reactors when tilting the

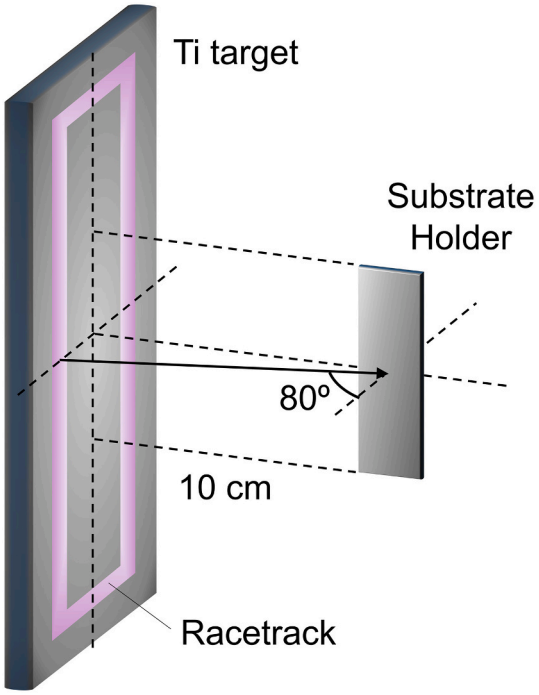

Fig. 3. Scheme of the experimental setup employed to carry out the depositions.

substrate holder. Indeed, in Fig. 1c–d the cross-sectional and top electron microscopy images of a TiO_2 thin film with thickness ~300 *nm*, deposited on a flat substrate using this configuration, are shown. There, it is apparent not only the clear nanocolumnar morphology of these films, but also the good agreement with the simulations presented in Fig. 1a–b.

The TiO_2 thin films were grown on patterned substrates: different patterns were defined on (100) oriented Si wafers by using substrate conformal imprint lithography (SCIL) with SiO_2 sol-gel as photoresist [46,47]. Then the residual layer of the imprinted photoresist was removed with inductively coupled plasma – reactive ion etching (ICP-RIE, Sentech SI 500) with a CHF_3 plasma. The structures were further transferred into Si substrate using reactive ion etching (RIE, Oxford Plasmalab 100) with a CF_4 plasma. After that, the imprinted sol-gel layer was removed by diluted HF solution. A total amount of 4 different patterns in 4 different scale lengths were imprinted, each with a size of $100 \times 100\ \mu m^2$, and separated 100 μm from each other. The four simple regular geometries were: i) lines perpendicular to the deposition flux (#Line1–#Line4), ii) lines parallel to the deposition flux (#ParLine1–#ParLine4), iii) cylindrical holes in a hexagonal pattern (#Hexa1–#Hexa4), and iv) cylindrical holes in a square pattern (#Square1–2 and #Mound1–2). These 4 geometries represent different possibilities of azimuthal orientation between the incident deposition flux and the elements defining the pattern: perpendicular (#Line1–4), parallel (#ParLine1–4), perpendicular and parallel (#Square 1–2 and #Mound1–2) as well as perpendicular, parallel and tilted (#Hexa1–4). Moreover, the 4 scale lengths were taken from few hundred nanometers to nearly 1 μm to check whether the film growth is affected in these scales. The central (flat) region of the substrate was taken as a reference for a growth on a flat surface topography. A scheme of the substrate pattern distribution appears in Fig. 4 (individual SEM images of each pattern appear in the supplementary information). The patterned substrates and the deposited films were analyzed by Field Emission Scanning Electron Microscopy (FESEM), using an FEI Verios 460 equipment at different magnification scales. Moreover, the Atomic Force Microscopy (AFM) technique was used prior to the film deposition to analyze the topography of the substrates with a Hysitron TS77 Select nanoindenter system manufactured by Bruker and available at the Complutense University of Madrid. In this way, the analysis of the topography of each pattern revealed that all carved parts were at least 100 nm deep, while the in-plane length of the lower carved regions in each substrate were measured and listed in Table 1. Overall, each

Table 1
Values of the typical length between the tallest regions of the substrate pattern, λ_0, along with the calculated and measured values of Δ_0, Δ_{FG} using Eqs. (2) and (3), respectively. Note that in all the patterns except #Mound1 the relation $\lambda_{min} = \lambda_{max} = \lambda_0$ holds. The values marked with the symbol (*) are presented and discussed in the Results and discussion section.

Pattern label	λ_0(nm)	Calculated Δ_0, Δ_{FG} (nm)	Experimental Δ_0,Δ_{FG} (nm)
#Line1, #ParLine1	550	~5900	$\Delta_0,\Delta_0 = \Delta_{FG} > 2000$
#Line2, #ParLine2	450	~4300	$\Delta_0,\Delta_0 = \Delta_{FG} > 2000$
#Line3, #ParLine3	350	~2900	$\Delta_0,\Delta_0 = \Delta_{FG} > 2000$
#Line4, #ParLine4	250	~1700	$\Delta_0 = \Delta_{FG}$~2000
#Hexa1	550	~5900	$\Delta_0,\Delta_0 = \Delta_{FG} > 2000$
#Hexa2	400	~3600	$\Delta_0,\Delta_0 = \Delta_{FG} > 2000$
#Hexa3	250	~1700	$1500 < \Delta_0 = \Delta_{FG} < 2000$
#Hexa4	150	~780	$500 < \Delta_0 = \Delta_{FG} < 1000$
#Square1	550	~5900	$\Delta_0 = \Delta_{FG} > 2000$
#Square2	400	~3600	$\Delta_0 = \Delta_{FG} > 2000$
#Mound1	λ_{min}~50*	Δ_0~140*	$100 < \Delta_0 < 300$,
	$\lambda_{max} = 250$	Δ_{FG}~1700	$1500 < \Delta_{FG} < 2000$
#Mound2	λ_{min}~150*	Δ_0~750*	$500 < \Delta_0 = \Delta_{FG} < 1000$
	$\lambda_{max} = 150$	Δ_{FG}~750	

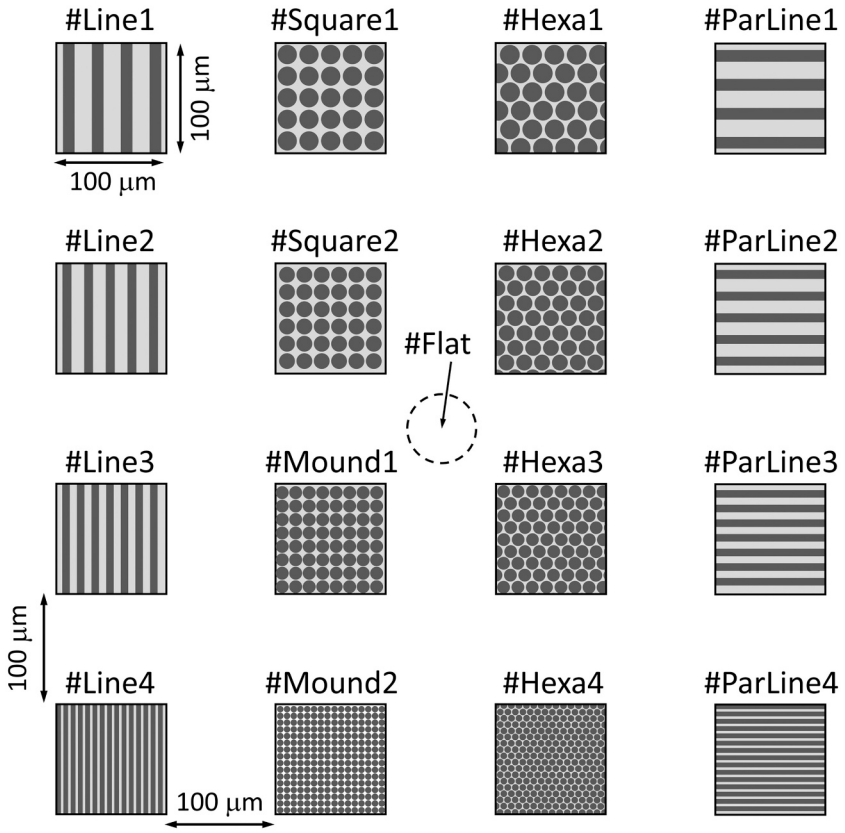

Fig. 4. Scheme of the substrate employed for the deposition, containing 4 patterns in 4 different scale lengths. The central part was taken as a reference for a film grown on a flat surface.

pattern possesses the following features:

- Lines Perpendicular to the deposition flux (#Line1–#Line4): These patterns contain carved 1D lines azimuthally perpendicular to the deposition flux. The typical size of the carved region for each pattern ranged from λ_0(*#Line*1)~550 nm to λ_0(*#Line*4)~250 nm (see Table 1). In order to illustrate these cases, in Fig. 5a the SEM image of pattern #Line1 taken at the border between the patterned and the flat regions of the substrate is displayed (the images of all #Line1–4 substrates appear in the supplementary information).
- Parallel Lines (#ParLine1–#ParLine4): These patterns are equal to #Line1–#Line4, but rotated 90°. In this way, the deposition flux is azimuthally parallel to the carved lines instead of perpendicular.
- Cylindrical Holes with Hexagonal distribution (#Hexa1–#Hexa4): This pattern consists of cylindrical holes with radius ranging from λ_0(*#Hexa*1)~550 nm to λ_0(*#Hexa*4)~150 nm (see Table 1), distributed according to a hexagonal geometry. This type of substrate is illustrated in Fig. 5b and c, where the top view SEM image of patterns #Hexa1 and #Hexa4, respectively, is displayed. Interestingly, in this latter case, the short typical distance between holes and their small radius induces numerous defects in the pattern, as it is apparent in Fig. 5c.
- Cylindrical Holes with Square Geometry (#Square1–#Square2): This pattern is made with cylindrical holes with radius λ_0(*#Square*1)~550 nm and λ_0(*#Square*2)~400 nm (see Table 1), in a square geometric distribution, as illustrated in Fig. 5d, where the SEM image of pattern #Square1 is displayed.
- Square geometry with mounds (#Mound1–#Mound2): this pattern emerged when carving the substrate with cylindrical holes in a square geometry, just like the #Square1–2 cases above. Yet, the holes were so close that they overlapped, being the small region in the center of four neighbor holes the only surviving tall region. In Fig. 6a–b a scheme of the hole distribution to produce such patterns, the SEM images of the substrates, and the AFM measurement of these structures are shown. In this way, the pattern #Mound1 represents the case where neighbor holes barely touch, resulting in the formation of a square distribution of mounds connected by smooth slopes (see AFM topography in Fig. 6a). The existence of these smooth slopes makes difficult to determine the size of the lower parts in the pattern. In the case of #Mound1, however, the value of λ_{max}(*#Mound*1)~250 nm can be determined (see Table 1), while the value of λ_{min} will be discussed later on. In case of pattern #Mound2 a similar behavior was found (see Fig. 6b), although now the mounds are smaller and present sharper slopes due to the overlapping of the holes. As in the #Mound1 case, the value λ_{max}(*#Mound*2)~150 nm was identified (see Table 1) while the value of λ_{min} will be discussed later on.

Given the patterns above, it is important to mention that, according to their topographical characterization, the carved regions in all the cases are defined by a single characteristic length, except in the #Mound1 and #Mound2 patterns. Moreover, in all the cases (see Figs. 5a–d and 6a–b) numerous small holes with diameter below 100 nm can be seen in both the region containing the pattern and the contiguous flat parts. These small holes appear as a side effect of the lithographic technique and have not been considered in the discussion. In any case, they clearly disappear from the film surface for film thicknesses above 50 nm (see results below).

Each TiO_2 deposition was progressively carried on using the same sample as substrate (i.e. the newly deposited film grows on top of the previous film), thus allowing to incrementally analyze the film topography with thickness. In this way, after each deposition, the sample was taken out of the reactor, its surface characterized, and put back inside for the following run. To better monitor the film growth, for each deposition the same flat Si substrate was placed next to the substrate containing the patterned regions, along with a fresh Si flat substrate to determine the incremental thickness. The deposition time was set to achieve progressive film thicknesses of ~50, 100, 300, 500, 1000, 1500 and 2000 nm, respectively. Depositions were stopped when the film thickness was 2000 nm, as it was enough to illustrate the different growth stages in most studied cases (see Section 4).

4. Results and discussion

In Fig. 7a the top view SEM images of the film grown on the flat substrate for thicknesses ranging from 50 to 2000 nm are shown. There, a clear granular morphology is depicted, typical of MS-OAD, where each grain represents the tip of a nanocolumn (see also Fig. 1b), whose size increases with thickness. From these images, the correlation length was obtained by calculating the first minimum of the height-height

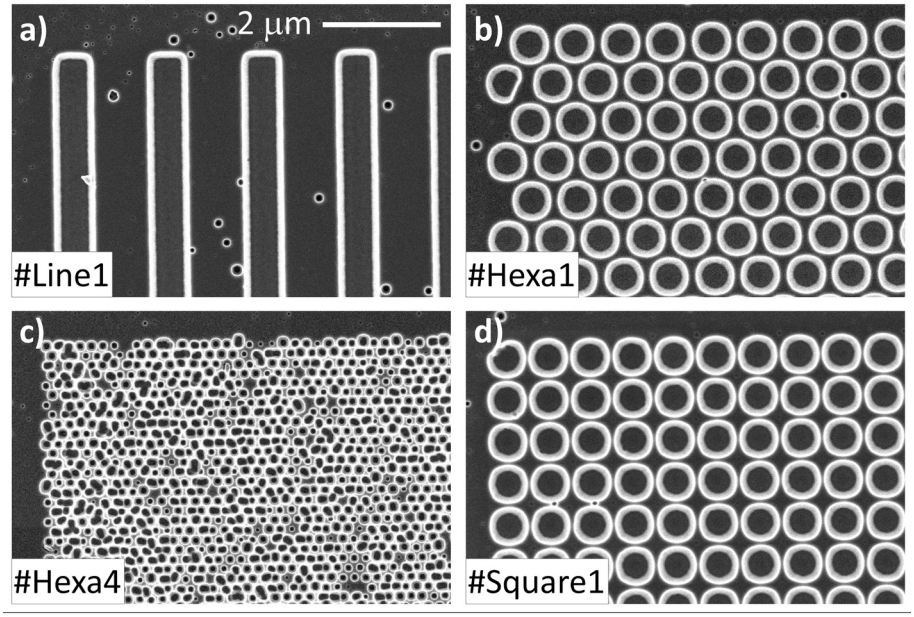

Fig. 5. SEM Images of four different patterns. a) #Line1, b) #Hexa1, c) #Hexa4, and d) #Square1.

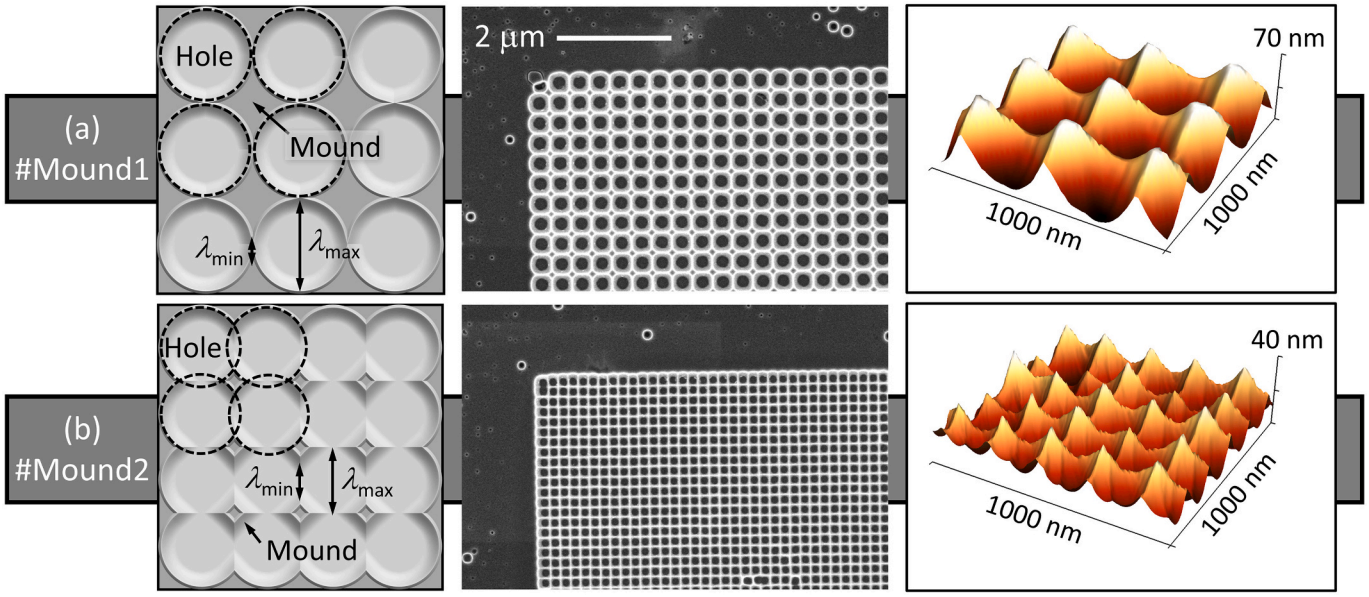

Fig. 6. Analysis of the patterns #Mound1–2, including a scheme on how the mounds are produced (left), SEM image (center) and AFM characterization of the surface (right). a) #Mound1, and b) #Mound2.

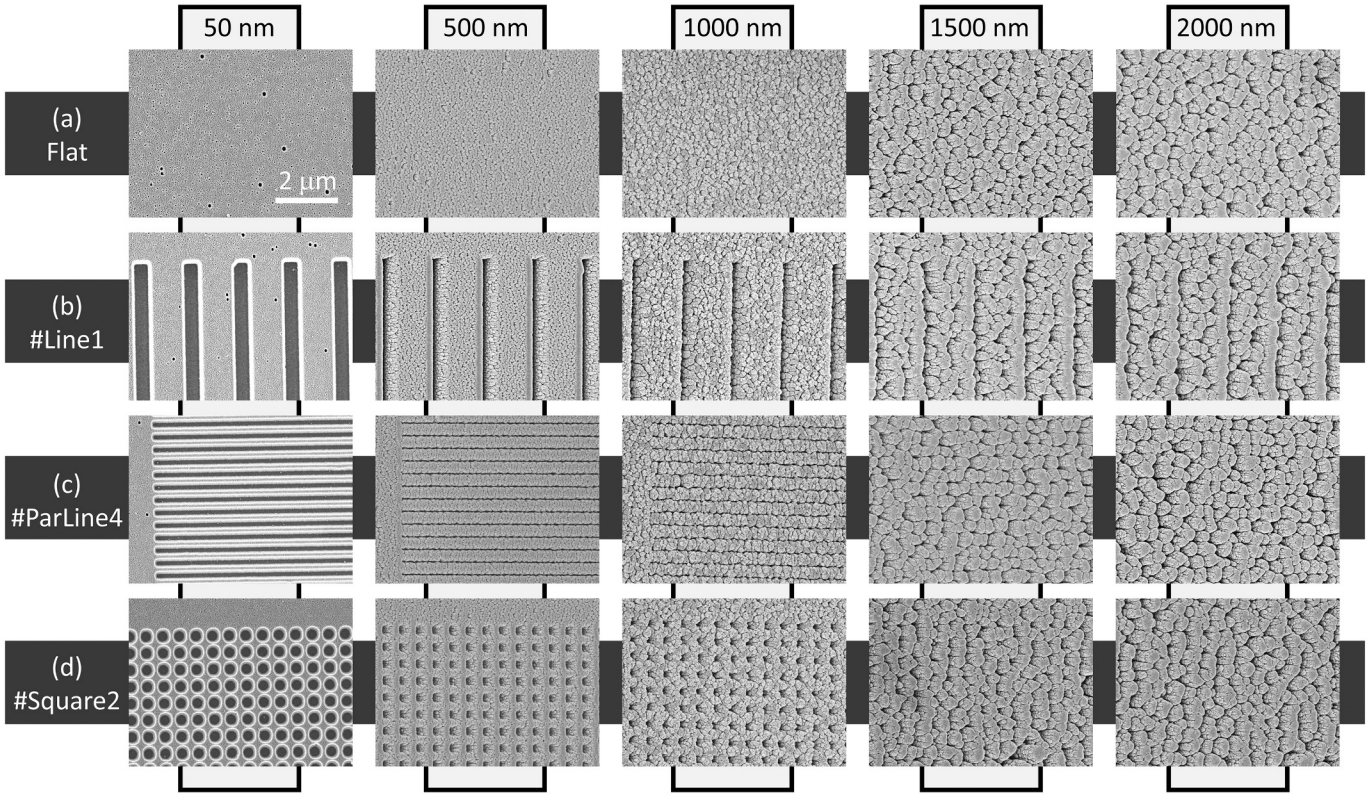

Fig. 7. Top view SEM of the deposited films as a function of thickness on different patterns. a) Flat surface, b) #Line1, c) #ParLine4, d) #Square2.

correlation function: the representation of λ_c as a function of thickness, Δ, is depicted in Fig. 8, where a clear power law between both quantities is found, in agreement with Eq. (1), with $\lambda_c = 2.12 \times \Delta^{0.64}$, being λ_c and Δ in nanometers. The relation between λ_c and Δ is of relevance as it provides the values of $C = 2.12$ and $z \sim 1/0.64 = 1.56$ in our conditions. Here, it is noteworthy that, in general, λ_c may show an anisotropic behavior, i.e. it may show a different trend depending on the particular direction under consideration. However, in this case, the value of λ_c has been checked to be rather isotropic, and therefore an averaged value of this parameter over the whole surface is presented. Next, the growth of the film deposited on each pattern, depending on its geometry, is discussed.

4.1. Growth on patterns #Line1–#Line4

In Fig. 7b the top SEM images taken for the films grown on #Line1

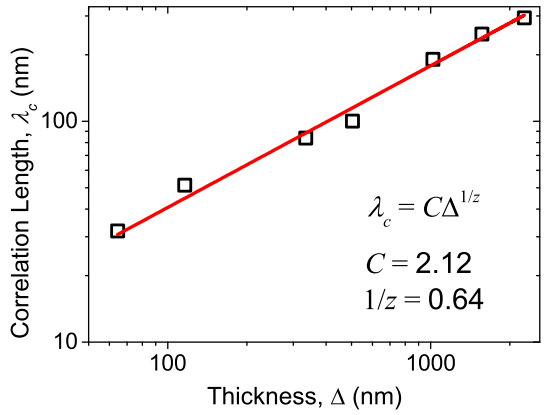

Fig. 8. Correlation length of the film deposited on a flat surface as a function of film thickness in a log-log representation. The numerical fit of the data to the power law in Eq. (1) is also included.

are shown for different values of Δ. For comparison purposes, the images were taken at the very border between the patterned and the flat regions of the substrate. At a glance, it can be noticed that the nanocolumns grow at the tallest parts of the substrate, in agreement with the height-based selective growth principle deduced in the previous section. Moreover, nanocolumns tend to disorganize with thickness, even though, in the studied range, the pattern is always visible from the top. This implies that the Oblivion Thickness has not been surpassed for film thicknesses below 2000 nm. In this regard, pattern #Line1 is defined by a single length for the lower pattern features, $\lambda_0 = 550$ nm, which according to Eq. (2) results in $\Delta_o \sim 5900$ nm, a value that agrees with the experiments (see Table 1). Fig. 9a shows a detail of this film morphology when its thickness is 100 nm: there, a small amount of deposited material can be seen inside the grooves, caused by those sputtered species that move as Brownian-like particles in the plasma, and that may arrive at the film surface from any possible direction, thus reaching the bottom of the grooves. The results for patterns #Line2–#Line4 are very similar to those of #Line1 and appear in the supplementary information.

4.2. Growth on patterns #ParLine1–#ParLine4

Fig. 7c shows a set of top SEM images of the films grown on the pattern #ParLine4 for different film thicknesses. These images illustrate the depositions on these geometries (the images for patterns #ParLine1–#ParLine3 are similar to those presented in Fig. 7c, and appear in the supplementary information). There, it can be appreciated again how the film mimics the tallest features of the pattern for small thicknesses, in agreement with the height-based selective growth principle. Moreover, it can be clearly seen how nanocolumns laterally spread out from tallest regions, progressively covering the grooves (i.e. the lower regions of the pattern), in a clear illustration of the fundamental mechanism discussed in the previous section. Remarkably, for a thickness of 1500 nm, it seems that the nanocolumns have completely covered the grooves, even though some order is still visible. The pattern seems to have vanished from the film surface for a thickness of 2000 nm, where the disorder is even higher, which agrees with the calculation of Δ_0 by Eq. (2), that results in $\Delta_0 \sim 1700$ nm (see Table 1). Fig. 9b presents a top view SEM image of the film grown on this pattern for a thickness of 100 nm. Again some deposition of material is noticeable at the bottom of the grooves, even though it is negligible in comparison with the amount of material deposited at the tallest regions.

4.3. Growth on patterns #Square1–#Square2

The top SEM images of the films deposited on the pattern #Square2 as a function of thickness are depicted in Fig. 7d, again taken in the border region between the pattern and the flat region of the substrate. This figure illustrates once more how the nanocolumnar arrangement accommodates on top of the tallest features of the substrate pattern. As in the previous cases, a small amount of deposited material is visible inside the holes (see detail of a hole for a film thickness of 100 nm in Fig. 9d), which can be again attributed to the existence of Brownian-like diffusive species in the plasma. Moreover, the Oblivion Thickness seems to be above 2000 nm, despite the fact that columns seem to become well disordered for the highest thicknesses, 1500 and 2000 nm. Yet, even for this last case they possess some evident alignment suggesting that the thickness remains below the Oblivion Thickness. This agrees with Eq. (2) where a value ~3600 nm is obtained (see Table 1). Similar results are

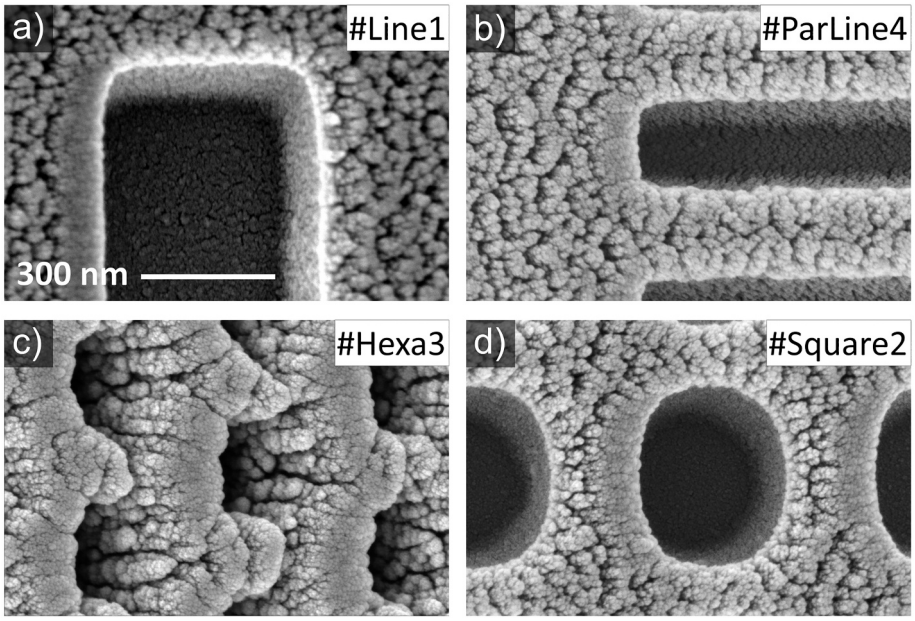

Fig. 9. Close-up SEM images of the deposited films a) #Line1 for a film thickness of 100 nm, b) #ParLine4 for a film thickness of 100 nm, c) #Hexa3 for a film thickness of 300 nm, d) #Square2 for a film thickness of 100 nm.

obtained for #Square1, which are displayed in the supporting information of this manuscript.

4.4. Growth on patterns #Hexa1–#Hexa4

The film growth on the pattern #Hexa3 is illustrated in Fig. 10a, where the top SEM images of the films with thicknesses ranging from 50 nm to 2000 nm are shown. There, it is clear that the tilted columnar growth mimics the tallest features of the substrate pattern up to a thickness of 1500 nm. Indeed, it is noticeable how the holes progressively close (see Fig. 9c for a detailed image of the holes for a film thickness of 300 nm) until the Oblivion Thickness is surpassed, an event that, according to Fig. 10a, must take place for a film thickness between 1500 and 2000 nm. Remarkably, Eq. (2) yields a value of ~1700 nm, which is in good agreement with the experiments (see Table 1). Similar results are obtained when the film grows on patterns #Hexa1 and #Hexa2, although this time the Oblivion Thickness is never reached in the studied range (see supplementary information for a complete set of images of the surface evolution of these films). The growth on pattern #Hexa4 is depicted in Fig. 10b, presenting a hexagonal array of cylindrical holes with numerous defects which, as commented before, are due to the substrate patterning process. In any case, the Oblivion Thickness is found for a thickness between 500 and 1000 nm, which agrees with the calculated value using Eq. (2) that gives away a value of ~780 nm (see Table 1).

4.5. Growth on patterns #Mound1–#Mound2

The evolution of the surface morphology of the films grown on pattern #Mound1 is depicted in Fig. 10c. Again, the top view SEM images are displayed as a function of the film thickness. Moreover, Fig. 11a shows a close-up detail of the morphology of this film for a thickness of 50 nm, 100 nm and 300 nm, respectively, where it can be observed how, for a thickness of 50 nm, the height-based selective growth does not only make nanocolumns develop at the apex of the mounds but also at the top parts of the slopes, forming cross-shaped periodic structures. Based on Fig. 11a the value λ_{min} can be now estimated as the distance between closest parts of the crosses, which gives λ_{min}~50 nm. This trend develops with thickness until individual elements touch one another and eventually merge (Fig. 11a), resulting in a characteristic square pattern, very similar to that found on pattern #Square2 in Fig. 7d. This suggests an Oblivion Thickness between 100 and 300 nm, in agreement with our calculations using Eq. (2), which, using the estimated value λ_{min}~50 nm, yields a value of Δ_0~140 nm (see Table 1). As in the previous cases, Fig. 10c shows that for increasing thicknesses, the nanocolumns progressively cover the holes defining the pattern until they disappear, giving rise to a free growth regime for a thickness between 1500 and 2000 nm. This result agrees with Eq. (3), that renders a value of Δ_{FG}~1700 nm for the λ_{max} value corresponding to this pattern (~250 nm - see Table 1).

The morphology of the films grown on the pattern #Mound2 is displayed in Fig. 10d as a function of thickness. There, it is remarkable the selective growth of the film on top of each mound, obtaining an ordered array structure with the shape of nanorods. This morphology defines the substrate for thicknesses below 1000 nm, at which the Oblivion Thickness is already surpassed. However, a closer look to these structures for a film thickness of 50 nm (see Fig. 11b) reveals an important aspect: contrary to the film grown on #Mound1, the sharper change of the slopes in this pattern causes the sole development of the apex of the mounds (Fig. 11b), indicating that in this case $\lambda_{min} = \lambda_{max} = \lambda_0$. In this way, the film morphology evolves as an array of well-ordered nanorods in a square geometrical arrangement, until these become well-packed for a thickness of 300 nm (Fig. 11b). This behavior continues even when the film is 500 nm thick in Fig. 10d, up to a thickness of 1000 nm for which the pattern is no longer visible on the film surface. This suggests that the Oblivion Thickness has been surpassed, in agreement

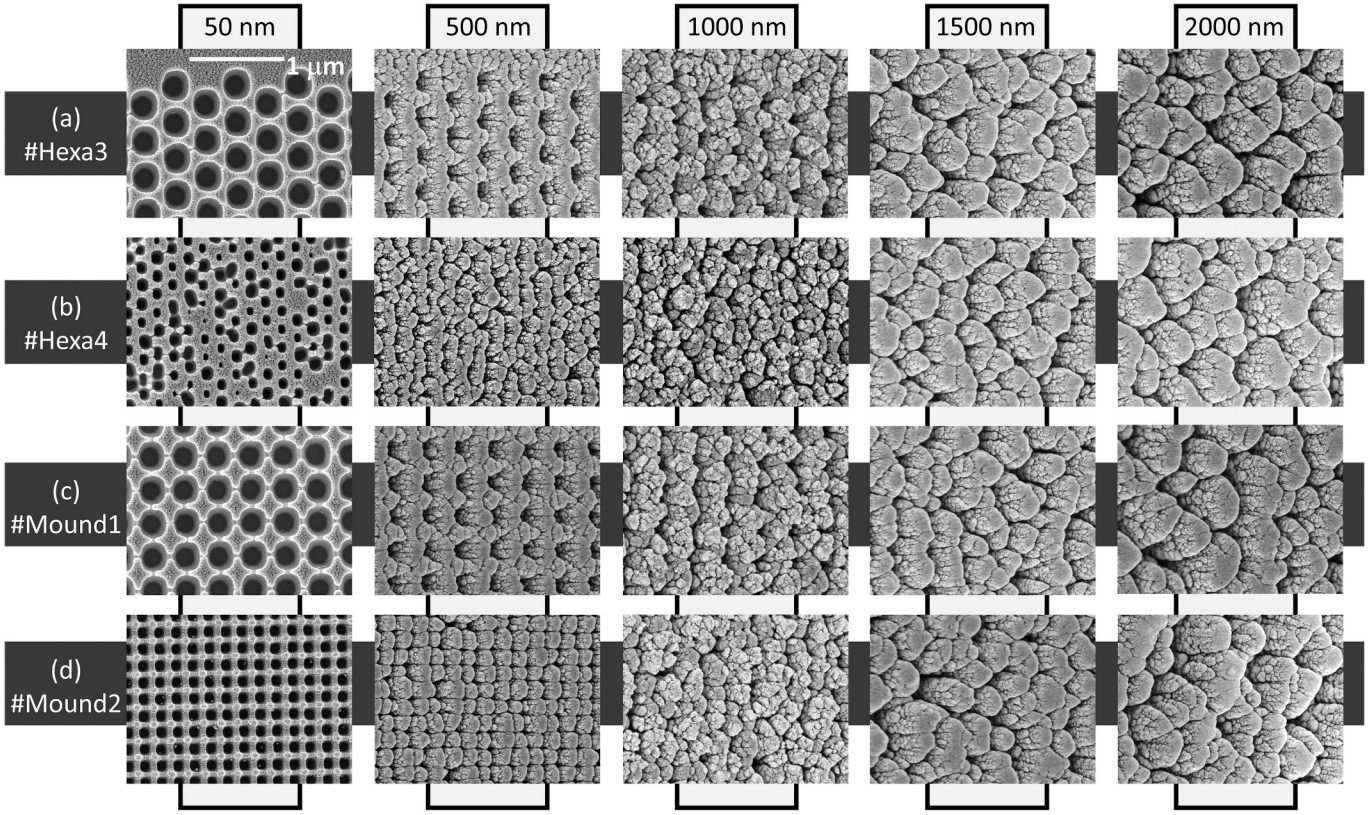

Fig. 10. Top view SEM of the deposited films as a function of thickness on different patterns. a) #Hexa3, b) #Hexa4, c) #Mound1, d) #Mound2.

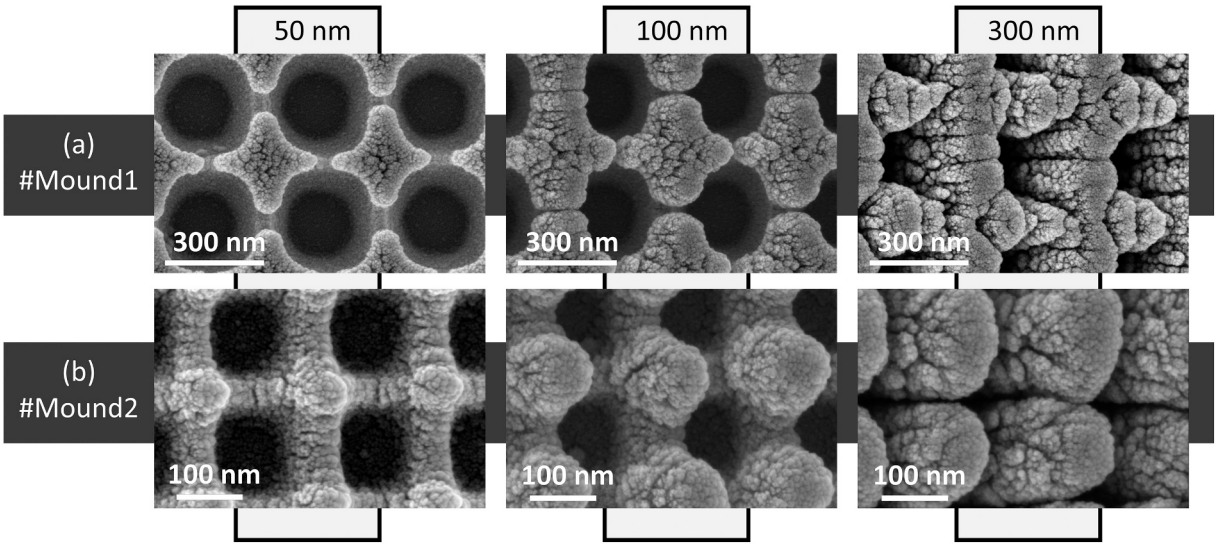

Fig. 11. Close-up SEM images of the films grown on patterns #Mound1 (a) and #Mound2 (b) for thicknesses 50, 100 and 300 nm.

with the calculated value using Eq. (2) of Δ_0~750 nm (see Table 1).

The experimental results above obtained on 4 different substrate patterns in 4 different scale lengths confirm the general framework developed in this paper and show that: i) the tallest substrate elements define the film topography in the initial stages of growth; ii) the nanocolumnar development promotes the progressive removal of shorter characteristic lengths of the pattern from the film surface; iii) Eq. (2), relating the Oblivion Thickness, the coarsening exponent and the shortest typical length between tallest elements in the pattern, has been tested against all the experimental cases finding a good agreement; and iv) the critical thickness to achieve a free growth regime agrees with Eq. (3), connecting this thickness with the biggest pattern feature size and the coarsening exponent. For simplicity, we have opted for a visual determination of the different growth regimes, although a Fourier or self-correlation analyses of the films' surfaces may illustrate these transitions quantitatively, similarly as it was done in ref. [28].

Based on the discussion above, it has been demonstrated that the existence of a substrate pattern strongly modifies the shadowing phenomenon and the collective growth of nanocolumns. Indeed, it has been shown that the film nanostructure can be tailored by substrate patterning for thicknesses below Δ_0 at oblique geometries. In this regard, the results presented herein provide the fundamental tools to perform such pattern design: the substrate topography, the required scale lengths, and the desired operational thicknesses of the films, conforming a basic framework to understand the interplay between substrate pattern and the nanocolumnar film growth. In this way, the ideas presented herein may have a strong impact on fields such as photonics, where geometrical order among nanorods (with typical distances in the range of the wavelength of the visible light) define the optical response of the material, or microfluidics, where it would be of relevance to grow thin films with tailored embedded channels or the construction of reservoirs enclosed in thin films for drug delivery in medical and biological applications, among others. Moreover, structures made in zig-zag can also be envisioned, or even multilayered well-ordered nanorod arrays (similar to those presented in Fig. 11b) for photonic applications. In this regard, the results presented in this paper present exciting new possibilities that will be analyzed in the near future.

5. Conclusions

The fundamental framework describing the interplay between substrate topography and thin film growth at oblique angles by magnetron sputtering is presented. A systematic analysis of the growth of TiO_2 thin films on 4 different lithographic patterned substrates (1D lines parallel and perpendicular to the deposition flux, and cylindrical hole structures in square or hexagonal geometries) in 4 different scale lengths has been carried out, corroborating the presented ideas. It is demonstrated that, besides classical nanocolumnar arrays, the oblique angle geometry promotes the growth of singular structures in the nanoscale when using wisely designed patterned substrates. As examples, well-ordered arrays of deposited crosses or cylindrical nanorods arranged according to square or hexagonal geometries have been obtained for film thicknesses of a few hundred nanometers.

Two general principles have been formulated describing the first stages of the film growth and the subsequent columnar development. With the help of a well-established growth model, the existence of a height-based selective growth principle has been demonstrated, by which the film mimics the pattern defined by the tallest elements of the substrate during the first stages of growth. This behavior is maintained up to a critical film thickness, the so-called Oblivion Thickness, above which the growth starts to structurally deviate up to a second critical thickness, the so-called Free Growth Thickness, above which the growth is independent of the features of the substrate. Based on these ideas, a mathematical relation has been deduced, linking the typical distances between the tallest elements of the pattern, the coarsening exponent defining the nanocolumnar growth, and the Oblivion and Free Growth Thicknesses. The existence of these growth regimes was experimentally illustrated by growing TiO_2 thin films by the magnetron sputtering technique at oblique angles on different patterns, corroborating the main ideas posed in this paper.

The results presented, and the fundamental framework describing the interplay between film and substrate features, open the possibility to employ substrate patterning as a feasible thin film nanostructuration technique. This would allow tailoring and optimizing the nanostructure of application-oriented materials by using a smart substrate pattern design, envisioning direct applications in fields as different as photonics, biomedicine, microfluidics and optics.

Supplementary data to this article can be found online at https://doi.org/10.1016/j.surfcoat.2022.128293.

CRediT authorship contribution statement

S. Muñoz-Piña: Investigation, Data Curation.
A.M. Alcaide: Formal analysis, Visualization.
B. Limones-Ahijón: Investigation.

M. Oliva-Ramírez: Investigation.
V. Rico: Investigation.
G. Alcalá: Investigation, Supervision.
M. U. González: Investigation.
J.M. García-Martín: Supervision.
R. Alvarez: Formal análisis, Software, Visualization.
D. Wang: Methodology, Resources.
P. Schaaf: Methodology, Resources.
A. R. González-Elipe: Supervision, Writing - Review & Editing.
A. Palmero: Conceptualization, Methodology, Writing - Original draft preparation.

Funding

The authors thank the financial support from MCIN/AEI/10.13039/501100011033 projects PID2019-110430GB-C21, PID2020-112620GB-I00, PID2020-114270RA-I00 and RTI2018-098117-B-C21 (also financed by FEDER Una manera de hacer europa), the Junta de Andalucía (PAIDI-2020 through projects P18-RT-3480 and P18-RT-6079, and through its 2019 PhD Researcher Hiring Program), the CSIC (2019AEP161 and 201860E050), the Regional Government of Madrid (project IND2017/IND-7668 and YEI contract PEJ-2019-AI/IND-14451 with support from FSE), the H2020-EU.1.2.1-FET OPEN program (grant 899352, project SOUNDofICE, and the EFRE Infra-Pro project ChAMP), and the University of Seville (VI PPIT-US).

The work is supported by the Deutsche Forschungsgemeinschaft (DFG, grant Scha 632/24, "Tailored Disorder" and Scha 632/27, "DFG-Gerätezentrum"). This work is also supported by the free state of Thuringia under grants 2015 FGI 0025 305 (FastμXRD) and B715-10009 (BioMacroNano2020), all co-financed by the European Union within the framework of the European Regional Development Fund (ERDF). The service from the MiNa Laboratory at IMN-CNM (CSIC), funded from CM (project S2018/NMT-4291 TEC2SPACE), MINECO (project CSIC13-4E-1794) and EU (FEDER, FSE), is also acknowledged.

Declaration of competing interest

The authors declare that they have no known competing financial interests or personal relationships that could have appeared to influence the work reported in this paper.

Acknowledgements

Support by the Center of Micro- and Nanotechnologies (ZMN), a DFG-funded core facility of TU Ilmenau, is gratefully acknowledged.

References

[1] H.B. Zhang, J.S. Cherng, Q. Chen, Recent progress on high power impulse magnetron sputtering (HiPIMS): the challenges and applications in fabricating VO2 thin film, AIP Adv. 9 (3) (2019), 035242, https://doi.org/10.1063/1.5084031.
[2] A. Garcia-Valenzuela, R. Alvarez, V. Rico, J. Cotrino, A.R. Gonzalez-Elipe, A. Palmero, Growth of nanocolumnar porous TiO2 thin films by magnetron sputtering using particle collimators, Surf. Coat. Technol. 343 (2018) 172, https://doi.org/10.1016/j.surfcoat.2017.09.039.
[3] J. Lu, Z. Chen, Z. Ma, F. Pan, L.A. Curtis, K. Amine, The role of nanotechnology in the development of battery materials for electric vehicles, Nat. Nanotechnol. 11 (2016) 1031, https://doi.org/10.1038/nnano.2016.207.
[4] D. Depla, S. Mahieu (Eds.), Reactive Sputter Deposition, Springer Series in Materials Science, Springer-Verlag, Berlin, Heildelberg, 2008. https://link.springer.com/book/10.1007/978-3-540-76664-3.
[5] J.E. Greene, Review article: tracing the recorded history of thin-film sputter deposition: from the 1800s to 2017, J. Vac. Sci. Technol. A 35 (5) (2017) 05C204, https://doi.org/10.1116/1.4998940.
[6] R.A. Surmenev, A review of plasma-assisted methods for calcium phosphate-based coatings fabrication, Surf. Coat. Technol. 206 (2012) 2035, https://doi.org/10.1016/j.surfcoat.2011.11.002.
[7] O. Tuna, Y. Selamet, G. Aygun, L. Ozyuzer, High quality ITO thin films grown by dc and RF sputtering without oxygen, J. Phys. D. Appl. Phys. 43 (2010), 055402, https://doi.org/10.1088/0022-3727/43/5/055402.
[8] A. Barranco, A. Borras, A.R. Gonzalez-Elipe, A. Palmero, Perspectives on oblique angle deposition of thin films: from fundamentals to devices, Prog. Mater. Sci. 76 (2016) 59, https://doi.org/10.1016/j.pmatsci.2015.06.003.
[9] B. Mohanty, B.D. Morton, A. Sinan Alagoz, T. Karabacak, M. Zou, Frictional anisotropy of tilted molybdenum nanorods fabricated by glancing angle deposition, Tribol. Int. 80 (2014) 216–221, https://doi.org/10.1016/j.triboint.2014.07.010.
[10] M.S. Rodrigues, J. Borges, M. Proença, P. Pedrosa, N. Martin, K. Romanyuk, A. L. Kholkin, F. Vaz, Nanoplasmonic response of porous Au-TiO2 thin films prepared by oblique angle deposition, Nanotechnology 30 (2019), 225701, https://doi.org/10.1088/1361-6528/ab068e.
[11] X. Xu, M.Pour Arab Yazdi, J.B. Sanchez, A. Billard, F. Berger, N. Martin, Exploiting the dodecane and ozone sensing capabilities of nanostructured tungsten oxide films, Sensor Actuat. B-Chem. 266 (2018) 773–783, https://doi.org/10.1016/j.snb.2018.03.190.
[12] J. Ollitrault, N. Martin, J.Y. Rauch, J.B. Sanchez, F. Berger, Improvement of ozone detection with GLAD WO3 films, Mater. Lett. 155 (2015) 1, https://doi.org/10.1016/j.matlet.2015.04.099.
[13] C. Sengstock, M. Lopian, Y. Motemani, A. Borgmann, C. Khare, P.J.S. Buenconsejo, T.A. Schildhauer, A. Ludwig, M. Koller, Structure-related antibacterial activity of a titanium nanostructured surface fabricated by glancing angle sputter deposition, Nanotechnology 25 (2014), 195101, https://doi.org/10.1088/0957-4484/25/19/195101.
[14] Y.J. Yoo, J.H. Lim, G.J. Lee, K.I. Jang, Y.M. Song, Ultra-thin films with highly absorbent porous media fine-tunable for coloration and enhanced color purity, Nanoscale 9 (2017) 2986, https://doi.org/10.1039/C6NR08475C.
[15] L. Yang, Y. Zhao, Y. Feng, J.S. Shan, X.Y. Liang, J. Huang, J.H. Mi, L.J. Wang, W. M. Shi, The influence of incident angle on physical properties of a novel back contact prepared by oblique angle deposition, Appl. Surf. Sci. 363 (2016) 252, https://doi.org/10.1016/j.apsusc.2015.12.017.
[16] D.B. Polat, O. Keles, The effect of copper coating on nanocolumnar silicon anodes for lithium ion batteries, Thin Solid Films 589 (2015) 543, https://doi.org/10.1016/j.tsf.2015.06.038.
[17] Y.J. Lee, Z.P. Yang, F.Y. Lo, J.J. Siao, Z.H. Xie, Y.L. Chuang, T.Y. Lin, J.K. Sheu, Slanted n-ZnO/p-GaN nanorod arrays light-emitting diodes grown by oblique-angle deposition, APL Mater. 2 (2014), 056101, https://doi.org/10.1063/1.4874455.
[18] J.J. Roa, V. Rico, M. Oliva-Ramirez, A.R. González-Elipe, E. Jiménez-Piqué, Nanoindentation and scratch resistance of multilayered TiO2-SiO2 coatings with different nanocolumnar structures deposited by PV-OAD, J. Phys. D. Appl. Phys. 49 (13) (2016), 135104, https://doi.org/10.1088/0022-3727/49/13/135104.
[19] V. Godinho, P. Moskovkin, R. Alvarez, J. Caballero-Hernández, R. Schierholz, B. Bera, J. Demarche, A. Palmero, A. Fernández, S. Lucas, On the formation of the porous structure in nanostructured a-Si coatings deposited by dc magnetron sputtering at oblique angles, Nanotechnology 25 (2014), 355705, https://doi.org/10.1088/0957-4484/25/35/355705.
[20] S. Liedtke, C. Gruener, J.W. Gerlac, B. Rauschenbach, Comparative study of sculptured metallic thin films deposited by oblique angle deposition at different temperatures, Beilstein J. Nanotechnol. 9 (2018) 954, https://doi.org/10.3762/bjnano.9.89.
[21] K. Kim, J.H. Park, H. Kim, J.K. Kim, E.F. Schubert, J. Cho, Energy bandgap variation in oblique angle-deposited indium tin oxide, Appl. Phys. Lett. 108 (2016), 041910, https://doi.org/10.1063/1.4940998.
[22] C. Lopez-Santos, R. Alvarez, A. Garcia-Valenzuela, V. Rico, M. Loeffler, A. R. Gonzalez-Elipe, A. Palmero, Nanocolumnar association and domain formation in porous thin films grown by evaporation at oblique angles, Nanotechnology 27 (2016), 395702, https://doi.org/10.1088/0957-4484/27/39/395702.
[23] R. Alvarez, J.M. Garcia-Martin, M. Macias-Montero, L. Gonzalez-Garcia, J. C. Gonzalez, V. Rico, J. Perlich, J. Cotrino, A.R. Gonzalez-Elipe, A. Palmero, Growth regimes of porous gold thin films deposited by magnetron sputtering at oblique incidence: from compact to columnar microstructures, Nanotechnology 24 (2013), 045604, https://doi.org/10.1088/0957-4484/24/4/045604.
[24] A. Palmero, H. Rudolph, F.H.P.M. Habraken, Generalized Keller-Simmons formula for nonisothermal plasma-assisted sputtering depositions, Appl. Phys. Lett. 89 (2006), 211501, https://doi.org/10.1063/1.2392830.
[25] D. Toledano, R.E. Galindo, M. Yuste, J.M. Albella, O. Sanchez, Compositional and structural properties of nanostructured ZnO thin films grown by oblique angle reactive sputtering deposition: effect on the refractive index, J. Phys. D. Appl. Phys. 46 (2013), 045306, https://doi.org/10.1088/0022-3727/46/4/045306.
[26] R. Mareus, C. Mastail, F. Angay, N. Brunetière, G. Abadias, Study of columnar growth, texture development and wettability of reactively sputter-deposited TiN, ZrN and HfN thin films at glancing angle incidence, Surf. Coat. Technol. 399 (2020), 126130, https://doi.org/10.1016/j.surfcoat.2020.126130.
[27] A. Besnard, N. Martin, C. Millot, J. Gavoille, R. Salut, Effect of sputtering pressure on some properties of chromium thin films obliquely deposited, IOP Conf. Ser: Mater. Sci. Eng. 12 (2010), 012015, https://doi.org/10.1088/1757-899X/12/1/012015.
[28] A. Garcia-Valenzuela, S. Muñoz-Piña, G. Alcala, R. Alvarez, B. Lacroix, A.J. Santos, J. Cuevas-Maraver, V. Rico, R. Gago, L. Vazquez, J. Cotrino, A.R. Gonzalez-Elipe, A. Palmero, Growth of nanocolumnar thin films on patterned substrates at oblique angles, Plasma Process. Polym. 16 (2) (2019) 1800135, https://doi.org/10.1002/ppap.201800135.
[29] S. Muñoz-Piña, A. Garcia-Valenzuela, E. Oyarzabal, J. Gil-Rostra, V. Rico, G. Alcala, R. Alvarez, F.L. Tabares, A. Palmero, A.R. Gonzalez-Elipe, Wetting and spreading of liquid lithium onto nanocolumnar tungsten coatings tailored through the topography of stainless steel substrates, Nucl. Fusion 60 (2020), 126033, https://doi.org/10.1088/1741-4326/abb53e.

[30] A. Dolatshahi-Pirouz, T. Jensen, T. Vorup-Jensen, Rikke Bech, J. Chevallier, F. Besenbacher, M. Foss, D.S. Sutherland, Synthesis of functional nanomaterials via colloidal mask templating and glancing angle deposition (GLAD), Adv. Eng. Mater. 12 (9) (2010) 899, https://doi.org/10.1002/adem.201000120.
[31] G.K. Kannarpady, K.R. Khedir, H. Ishihara, J. Woo, O.D. Oshin, S. Trigwell, C. Ryerson, A.S. Biris, Controlled growth of self-organized hexagonal arrays of metallic nanorods using template-assisted glancing angle deposition for superhydrophobic applications, ACS Appl. Mater. Interfaces 3 (7) (2011) 2332, https://doi.org/10.1021/am200251n.
[32] Y. Lim, S. Hong, J. Bae, H. Yang, Y.B. Kim, Influence of deposition temperature on the microstructure of thin-film electrolyte for SOFCs with a nanoporous AAO support structure, Int. J. Hydrog. Energy 42 (2017) 10199, https://doi.org/10.1016/j.ijhydene.2017.03.148.
[33] F. Chen, A.H. Kitai, Growth of nanoporous silicon dioxide thin films using porous alumina substrates, Thin Solid Films 517 (2008) 622, https://doi.org/10.1016/j.tsf.2008.07.009.
[34] P.L. Johnson, D. Teeters, Formation and characterization of SnO2 nanobaskets, Solid State Ionics 177 (2006) 2821, https://doi.org/10.1016/j.ssi.2006.01.029.
[35] G.Q. Ding, W.Z. Shen, M.J. Zheng, D.H. Fan, Synthesis of ordered large-scale ZnO nanopore arrays, Appl. Phys. Lett. 88 (2006), 103106, https://doi.org/10.1063/1.2182025.
[36] G. Sievers, T. Vidakovic-Koch, C. Walter, F. Steffen, S. Jakubith, A. Krut, Ultra-low loading Pt-sputtered gas diffusion electrodes for oxygen reduction reaction, J. Appl. Electrochem. 48 (2018) 221, https://doi.org/10.1007/s10800-018-1149-7.
[37] V. Perekrestov, A. Kornyushchenko, V. Natalich, S. Ostendorp, G. Wilde, Formation of porous nickel nanosystems using alumina membranes as templates for deposition, Mater. Lett. 153 (2015) 171, https://doi.org/10.1016/j.matlet.2015.03.141.
[38] A.I. Pereira, P. Pérez, S.C. Rodrigues, A. Mendes, L.M. Madeira, C.J. Tavares, Deposition of Pd–Ag thin film membranes on ceramic supports for hydrogen purification/separation, Mater. Res. Bull. 61 (2015) 528, https://doi.org/10.1016/j.materresbull.2014.10.055.
[39] S.-K. Ryi, J.-S. Park, K.-R. Hwang, D.-W. Kim, H.-S. An, Pd-cu alloy membrane deposited on alumina modified porous nickel support (PNS) for hydrogen separation at high pressure, J. Chem. Eng. 29 (2012) 59, https://doi.org/10.1007/s11814-011-0127-0.
[40] A. Gutiérrez-Delgado, G. Domínguez-Cañizares, J.A. Jiménez, I. Preda, D. Díaz-Fernández, F. Jiménez-Villacorta, G.R. Castro, J. Chaboy, L. Soriano, Hexagonally-arranged-nanoporous and continuous NiO films with varying electrical conductivity, Appl. Surf. Sci. 276 (2013) 832, https://doi.org/10.1016/j.apsusc.2013.04.007.
[41] D.K. Maurya, A. Sardarinejad, K. Alameh, Recent developments in R.F. magnetron sputtered thin films for pH sensing applications—an overview, Coatings 4 (2014) 756, https://doi.org/10.3390/coatings4040756.
[42] H.S. Al-Salman, M.J. Abdullah, Preparation of ZnO nanostructures by RF-magnetron sputtering on thermally oxidized porous silicon substrate for VOC sensing application, Measurement 59 (2015) 248, https://doi.org/10.1016/j.measurement.2014.08.011.
[43] M. Pelliccione, T.-M. Lu, Evolution of Thin Film Morphology, Springer-Verlag, Berlin, 2008. https://link.springer.com/book/10.1007/978-0-387-75109-2.
[44] A.L. Barabàsi, H.E. Stanley, Fractal Concepts in Surface Growth, Cambridge University Press, Cambridge, England, 1995, https://doi.org/10.1017/CBO9780511599798.
[45] R. Alvarez, S. Muñoz-Piña, M.U. González, I. Izquierdo-Barba, I. Fernández-Martínez, V. Rico, D. Arcos, A. García-Valenzuela, A. Palmer, M. Vallet-Regi, A. R. González-Elipe, José M. García-Martin, Antibacterial nanostructured Ti coatings by magnetron sputtering: from laboratory scales to industrial reactors, Nanomaterials 9 (2019) 1217, https://doi.org/10.3390/nano9091217.
[46] R. Ji, M. Hornung, M.A. Verschuuren, R. van de Laar, J. van Eekelen, U. Plachetka, M. Moeller, C. Moormann, UV enhanced substrate conformal imprint lithography (UV-SCIL) technique for photonic crystals patterning in LED manufacturing, Microelectron. Eng. 87 (5–8) (2010) 963, https://doi.org/10.1016/j.mee.2009.11.134.
[47] D. Wang, R. Ji, P. Schaaf, Formation of precise 2D Au particle arrays via thermally induced dewetting on pre-patterned substrates, Beilstein J. Nanotechnol. 2 (2011) 318, https://doi.org/10.3762/bjnano.2.37.